Molecular Microbiology

WILEY

RESEARCH ARTICLE OPEN ACCESS

An Extracellular, Ca^{2+}-Activated Nuclease (EcnA) Mediates Transformation in a Naturally Competent Archaeon

Dallas R. Fonseca[1] | Leslie A. Day[1] | Kathryn K. Crone[2] | Kyle C. Costa[1]

[1]Department of Plant and Microbial Biology, University of Minnesota, Saint Paul, Minnesota, USA | [2]Department of Biochemistry, Molecular Biology, and Biophysics, University of Minnesota, Saint Paul, Minnesota, USA

Correspondence: Kyle C. Costa (kcosta@umn.edu)

Received: 17 January 2024 | **Revised:** 9 August 2024 | **Accepted:** 11 August 2024

Funding: This work was supported by National Science Foundation, MCB-2148165.

Keywords: competence | DNA cleavage | DNA repair | DNA transformation | horizontal gene transfer | *Methanococcus* | nucleic acid denaturation

ABSTRACT

Transformation, the uptake of DNA directly from the environment, is a major driver of gene flow in microbial populations. In bacteria, DNA uptake requires a nuclease that processes dsDNA to ssDNA, which is subsequently transferred into the cell and incorporated into the genome. However, the process of DNA uptake in archaea is still unknown. Previously, we cataloged genes essential to natural transformation in *Methanococcus maripaludis*, but few homologs of bacterial transformation-associated genes were identified. Here, we characterize one gene, MMJJ_16440 (named here as *ecnA*), to be an extracellular nuclease. We show that EcnA is Ca^{2+}-activated, present on the cell surface, and essential for transformation. While EcnA can degrade several forms of DNA, the highest activity was observed with ssDNA as a substrate. Activity was also observed with circular dsDNA, suggesting that EcnA is an endonuclease. This is the first biochemical characterization of a transformation-associated protein in a member of the archaeal domain and suggests that both archaeal and bacterial transformation initiate in an analogous fashion.

1 | Introduction

Natural transformation is a mechanism by which microbes acquire new DNA directly from the environment. First observed in *Streptococcus pneumoniae* (Avery, Macleod, and McCarty 1944) (previously referred to as *pneumococcus*), natural transformation has been investigated since the 1940s in numerous bacteria. Across all known naturally transformable bacteria, a series of operational steps appear to be common (Pimentel and Zhang 2018; Averhoff et al. 2021). First, a cell must enter into a physiological state known as the competent state, typically through sensing of environmental stimuli such as quorum sensing in *Vibrio* species (Sun et al. 2013) or in response to starvation in *Bacillus* species (Schultz et al. 2009; Maier 2020). Once in the competent state, extracellular appendages (typically Type IV-like filaments) extend from the cell surface to bind extracellular DNA (Piepenbrink 2019). Pili then retract to localize DNA to the cell surface where the incoming DNA is partially degraded into ssDNA by an extracellular nuclease (Puyet, Greenberg, and Lacks 1990; Provvedi, Chen, and Dubnau 2001) for transport through the membrane transporter ComEC (Pimentel and Zhang 2018). Once inside the cell, ssDNA must be protected from intracellular nucleases through the binding of ssDNA-binding proteins, such as RecA, which subsequently drives recombination into the chromosome (Johnston et al. 2023).

While this series of steps is functionally conserved in several bacteria, an understanding of how archaea acquire DNA through natural transformation is lacking (Gophna and Altman-Price 2022). Transformation has been observed in several archaea (Worrell et al. 1988; Patel et al. 1994; Sato et al. 2003; Lipscomb et al. 2011; Wagner et al. 2017; Fonseca et al. 2020); however, homologs to many of the known bacterial genes cannot be identified in these organisms, suggesting that archaea may

have independently evolved a system for the uptake of exogenous DNA. Previously, we cataloged several genes essential to natural transformation in the archaeon *Methanococcus maripaludis* (Fonseca et al. 2020, 2023). Importantly, we identified several predicted membrane proteins important to DNA uptake.

Here, we focus on the characterization of MMJJ_16440, a predicted extracellular nuclease, to determine its role in DNA transfer in archaea. We show that MMJJ_16440 degrades several physiologically relevant forms of DNA (circular dsDNA, linear dsDNA, and linear ssDNA). Furthermore, it is Ca^{2+}-activated, similar to characterized biofilm-modulating nucleases in bacteria (Kiedrowski et al. 2014). We compared activity with ssDNA and dsDNA and observed a higher degradation rate with ssDNA, suggesting that ssDNA is the preferred substrate. Taken together, these data suggest that as DNA is introduced to whole cells, MMJJ_16440 separates dsDNA into ssDNA (either through nicking or a double-strand break) and degrades one strand before (or coincidently to) the other entering the cell. To be maintained, ssDNA must be repaired or integrated into the genome, meaning that the steps for transformation in archaea are analogous to those in bacteria.

2 | Results

2.1 | MMJJ_16440 Is Essential for Transformation

MMJJ_16440 is essential to natural transformation in *M. maripaludis* strain JJ (Fonseca et al. 2023). MMJJ_16440 is predicted to be a nuclease and based on sequence identity (Price and Arkin 2017) is homologous to two nucleases from *Staphylococcus aureus*, Nuc and Nuc2 (encoded in ORFs SAUSA300_0776 and SAUSA300_1222, respectively). Additionally, analysis of the MMJJ_16440 amino acid sequence with signalP 6.0 (Teufel et al. 2022) suggested that the protein contains an N-terminal Sec/SPII signal peptide (Figure S1; File S3). This signal peptide processing and anchoring is well-characterized in bacteria, but the archaeal machinery for Sec/SPII processing remains unknown (Pohlschroder et al. 2018). In bacteria, the Sec/SPII signal peptide is loaded into the Sec pore, then a cleavage event occurs between two amino acids releasing the protein into the environment. A cysteine following the cleavage site is then post-translationally modified with a lipid that anchors the protein in the membrane. Based on the signalP prediction and how processing occurs in bacteria, we hypothesized that a cysteine (C18) at the end of the predicted Sec/SPII signal of MMJJ_16440 is the site of lipid anchoring. To test this, we generated a strain carrying a MMJJ_16440 C18S mutation and observed an order of magnitude reduction in transformation efficiency (Figure 1A). This suggests that C18 is not essential for activity, but putative membrane anchoring may enhance transformation efficiency.

2.2 | MMJJ_16440 Is Homologous to Nuc and Nuc2

We performed a phylogenetic reconstruction of MMJJ_16440 against five characterized bacterial nucleases to generate predictions about its properties. We selected nucleases that are known to be involved in DNA processing during bacterial transformation such as EndA from *S. pneumoniae* (Puyet, Greenberg, and Lacks 1990) and NucA from *Bacillus subtilis* (Provvedi, Chen,

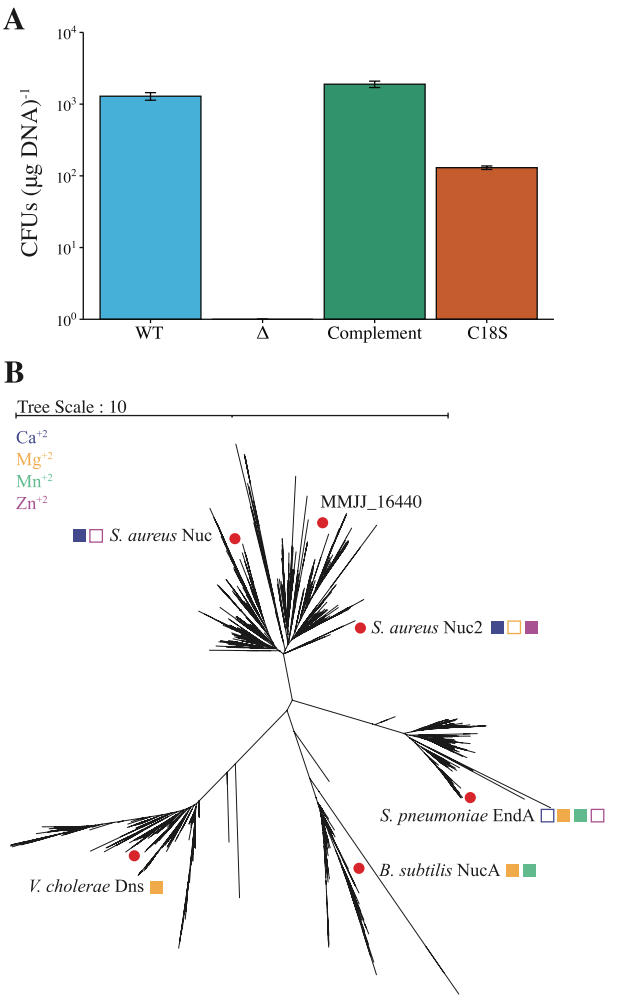

FIGURE 1 | MMJJ_16440 is a predicted membrane-bound nuclease essential to transformation in *Methanococcus maripaludis*. (A) Transformation efficiency of *M. maripaludis* nuclease strains. Cells were transformed with either pLW40neo (WT and Δ) or pLW40 (Complement and C18S). WT refers to our WT strain KC13 (Fonseca et al. 2023). Δ refers to KC13ΔMMJJ_16440 (KC89). Complement refers to KC13ΔMMJJ_16440 + pLW40neo-MMJJ_16440 (KC137) which expresses MMJJ_16440 under the high expression P*hmv* promoter (Gardner and Whitman 1999). C18S refers to KC13ΔMMJJ_16440C18S (KC143) which is under the same high expression promoter as the complement but is predicted to remove a putative lipid modification, thus releasing it from the cell surface once secreted through the Sec pore. Data are averages from three independent experiments, and error bars represent one standard deviation around the mean. (B) Phylogenetic reconstruction of selected nucleases. Six representative nucleases were chosen for evolutionary analysis as described in the text. The tree was generated using FastTree (Price, Dehal, and Arkin 2009, 2010) and visualized in Newick format using the Interactive Tree of Life (iTol) web browser (Letunic and Bork 2021). Five of these nucleases are cation dependent. Filled boxes refer to a cation that activated the nuclease, and empty boxes refer to tested cations that either exhibited no nuclease activity or inhibition of activity. If boxes are absent, the respective cation was not tested.

and Dubnau 2001). Both nucleases are membrane-bound and require divalent cations for activity, namely Mg^{2+} or Mn^{2+} for EndA (Moon et al. 2011), or Mn^{2+} (with partial activity noted

with Mg^{2+}) for NucA (Vosman et al. 1987, 1988; van Sinderen, Kiewiet, and Venema 1995). Next, we chose Nuc and Nuc2 from *S. aureus* as the closest characterized sequence hits (~34%–38% identical to MMJJ_16440). Nuc and Nuc2 are both thermostable and Ca^{2+}-activated (with partial activity detected in Nuc2 with Zn^{2+}) but have different cellular localization. Nuc is secreted and released into the supernatant while Nuc2 is membrane-bound (Kiedrowski et al. 2014). While *S. aureus* was thought to be incapable of natural transformation, recent studies have shown DNA uptake during biofilm maturation or DNA damage (Cordero et al. 2022; Maree et al. 2022). It is unclear whether Nuc or Nuc2 is important for transformation in *S. aureus*. Finally, we used the sequence of an extracellular nuclease from *Vibrio cholera*, Dns, which functions in nucleotide scavenging (Lo Scrudato and Blokesch 2012) as it is a similar nuclease but with a distinct biological function.

We recovered the top 500 matches from a BlastP search on each nuclease. After merging and deduplication (based on name and sequence), 1959 sequences were used in a phylogenetic reconstruction (Figure 1B). We observed four independent clusters of sequences, with MMJJ_16440, Nuc, and Nuc2 clustering together. While several of the nucleases can have activity activated by multiple divalent cations, a general trend was that the Ca^{2+}-activated nucleases clustered separately from the Mg^{2+}/Mn^{2+}-activated nucleases (Figure 1B). Based on its position in this tree, we hypothesized that MMJJ_16440 is Ca^{2+}-activated, similar to Nuc and Nuc2.

2.3 | MMJJ_16440 Is Extracellular

Given that MMJJ_16440 is predicted to be secreted through a Sec/SPII signal, we sought to determine its localization. We were unable to visualize MMJJ_16440 via Coomassie staining, western blot, and mass spectrometry methods in any strains tested, suggesting that the native protein is present below the detection limit of these methods. However, using a FRET-based assay described in the characterization of Nuc and Nuc2 (Kiedrowski et al. 2011, 2014), we were able to observe nuclease activity on the cell surface. Briefly, the assay utilizes an ssDNA oligo where the 5′ end is modified with a Cy3 fluorophore and the 3′ end is modified with Black Hole Quencher 2. When intact, the signal from Cy3 is quenched by proximity to the quencher. In the presence of an endonuclease, the Cy3 fluorophore is released from the quencher resulting in detectable fluorescence over time.

We were unable to detect activity in WT cells but observed activity in whole cells expressing MMJJ_16440 in *trans* under the control of the high expression P*hmv* promoter (Gardner and Whitman 1999) (Figure 2A). Activity was also observed in supernatants from cells expressing the C18S variant (Figure 2B). Should MMJJ_16440 be processed by machinery like the bacterial Sec/SPII system, these data suggest that the inability to add a lipid modification to the protein results in release from the cell surface, but further characterization into the mechanism of lipidification is warranted.

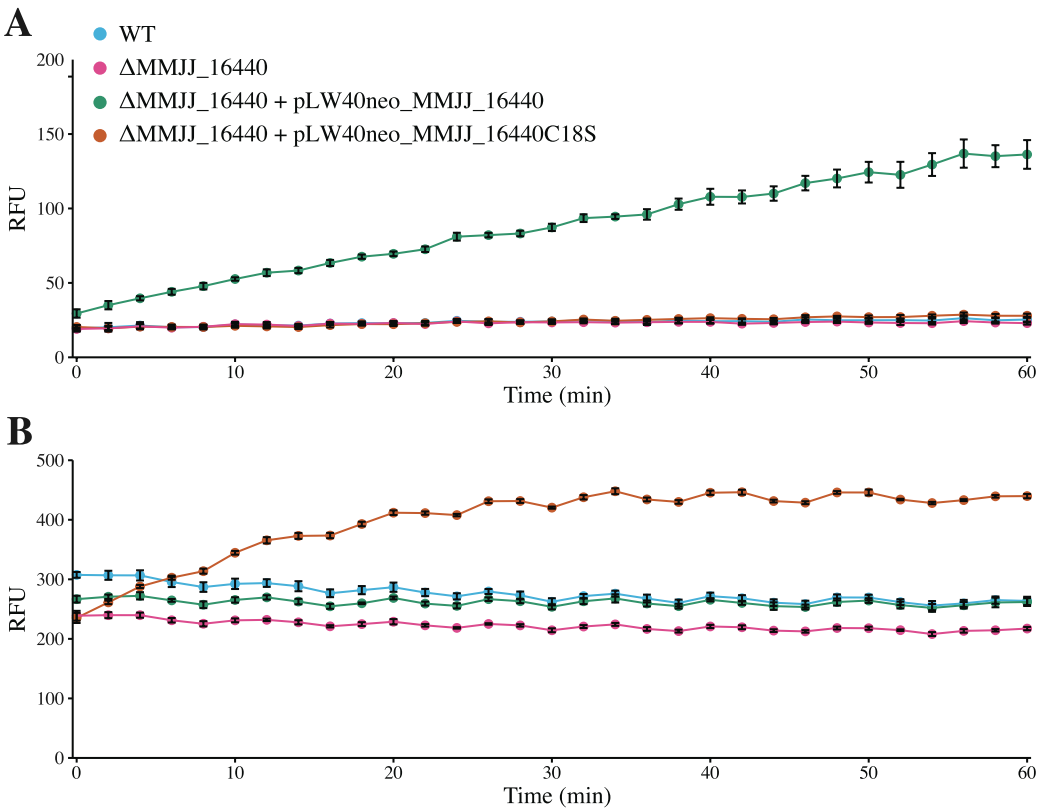

FIGURE 2 | FRET-based nuclease assay on *Methanococcus maripaludis* whole cells and secretome. (A) Fluorescence of *M. maripaludis* cells mixed with FRET-based DNA oligo. (B) Fluorescence of *M. maripaludis* supernatants mixed with FRET-based DNA oligo. Data are averages of four independent replicates and error bars represent one standard deviation around the mean. RFU, relative fluorescence units.

2.4 | Purified MMJJ_16440 Is a Ca^{2+}-Activated Nuclease

To characterize MMJJ_16440, we purified the protein to homogeneity. We were unable to recover protein from the native host, presumably either due to low abundance or the membrane-bound nature of the enzyme. Using a heterologous expression system in *Escherichia coli*, we expressed a histidine tagged variant of the nuclease domain (MMJJ_16440Δ2-18) under an inducible promoter, but this construct also failed to yield detectable protein, possibly due to insolubility of the protein. To overcome this, we generated a maltose-binding protein (MBP) fusion with a TEV protease cleavage site between the MBP and MMJJ_16440 domains. With this approach, we isolated >95% pure protein (Figure 3A, lane b) with an average yield of ~5 mg per liter across purifications (as determined by Bradford assay (Bradford 1976)). Treating MBP-MMJJ_16440Δ2-18 protein with TEV protease resulted in a mixed population of both nuclease and MBP proteins (Figure 3A, lane c). MMJJ_16440Δ2-18 could be further purified by gel filtration chromatography, but yields were often too low at 90% purity to perform subsequent characterization. We also generated MBP alone as a control for all experiments (Figure 3A, lane a).

To test purified protein for nuclease activity, we performed reactions in the wash buffer used in the whole-cell FRET-based assay. Both the MBP-MMJJ_16440Δ2-18 protein and the MMJJ_16440Δ2-18 protein mixed population had detectable nuclease activity on a plasmid substrate (pCRUptNeo). Of note, when performing all agarose-based nuclease assays, we provided an excess amount of DNA substrate for visualization to observe whether any stable intermediates were being generated, but we saw no evidence of such. Furthermore, supercoiled DNA was not resistant to DNA degradation, suggesting that MMJJ_16440 can perform double-strand breaks to generate linear dsDNA or can nick the plasmid to generate relaxed circular DNA.

To determine whether Mg^{2+} or Ca^{2+} is essential for activity, we first assayed for nuclease activity in 10 mM Tris–HCl (pH 7.5), and no activity was observed. We then added $CaCl_2$ or $MgCl_2$ (0.5 or 25 mM, final concentrations, respectively) and only observed nuclease activity in Ca^{2+}-containing buffer. Furthermore, activity was significantly higher in 10 mM Tris–HCl (pH 7.5) + 0.5 mM $CaCl_2$ than in wash buffer (Figure 3C). These data suggest that MMJJ_16440 is a Ca^{2+}-activated nuclease, consistent with phylogenetic clustering with Nuc and Nuc2. Of note, we did not observe any differences in activity between the fused MBP-MMJJ_16440Δ2-18 and the MMJJ_16440Δ2-18 mixed prep. Given these equal activities, we decided to perform all remaining characterizations with MBP-MMJJ_16440Δ2-18 given that it was generally more stable and protein yield was significantly higher by omitting the TEV cleavage step of the purification.

2.5 | MMJJ_16440 Shares Some of the Conserved Active Site Residues of Nuc

To further validate that the activity we observed in vitro after heterologous expression in *E. coli* was due the activity of MMJJ_16440 and not rare contaminants in our purifications, we performed structural and amino acid alignments of MMJJ_16440 against Nuc and Nuc2 to identify candidate catalytic residues for point mutagenesis studies. In Kiedrowski et al. (2014), the authors performed a Phyre2 analysis of Nuc2 threaded onto the crystal structure of Nuc (PDB-1SNO) and note a high confidence structural similarity in the matured proteins. Similarly, subjecting MMJJ_16440 to a search in Phyre2 (Kelley et al. 2015), the crystal structure of Nuc (PDB-1SNO) was used as the template to generate the top model (100.0% confidence at 69% coverage). Given this similarity, we performed an amino acid alignment (Clustal omega (Madeira et al. 2022)) of all three proteins, Nuc, Nuc2, and MMJJ_16440, to determine whether the catalytic residues known for Nuc are conserved. A representation of this alignment is provided as Figure 4A.

There are nine catalytic residues for Nuc (Cotton, Hazen, and Legg 1979; Kiedrowski et al. 2014), seven of which are conserved in Nuc2. MMJJ_16440 also shares seven conserved catalytic residues, but only six of these are conserved across all three proteins. Structural studies of Nuc complexed with the small molecule thymidine 3′,5′–bisphosphate (pdTp) suggest that some of the residues are involved in coordinating the Ca^{2+} cation, while others are involved in the stabilization of the phosphate of pdTp (Cotton, Hazen, and Legg 1979). Given that we have shown Ca^{2+} to be required for MMJJ_16440 activity, we chose to focus on residues that are implicated in binding the phosphate. Two residues that were of interest to us were MMJJ_16440 R131 and Y129 as these residues seem to exclusively interact with the nucleotide and are conserved across all three proteins. To test whether these residues are essential to MMJJ_16440 catalytic activity in vitro, we heterologously expressed the nuclease domains of MMJJ_16440 containing R131A or Y129F mutations in *E. coli*, purified these enzymes, (SDS-PAGE analysis of purity is provided as Figure S2) then subjected them to our agarose-based nuclease assay. Interestingly, we observed that the R131A mutation resulted in complete loss of detectable nuclease activity while the Y129F mutation resulted in the same level of activity as wild type (Figure 4). This suggests that the nuclease activity observed in our previous assay is in fact due to the activity of MMJJ_16440 and not a rare *E. coli* contaminant. This also suggests that MMJJ_16440 may use a similar, but not identical mechanism to that proposed for Nuc (Cotton, Hazen, and Legg 1979).

2.6 | MMJJ_16440 Degrades Both dsDNA and ssDNA

We next determined whether MMJJ_16440 displayed a DNA substrate preference. We changed the plasmid substrate to pLW40, another circular dsDNA plasmid of larger size (10.3 kb vs. 6.6 kb) and different composition (average GC content of 37% vs. 48% for pCRUptNeo). Additionally, pCRUptNeo is a suicide vector while pLW40 is a self-replicating plasmid. While both plasmids are transformation substrates (Fonseca et al. 2020, 2023), the ultimate fate of transformed DNA is different, where pCRUptNeo-derived vectors must be integrated into the chromosome and pLW40 is maintained independently. Interestingly, within the same reaction time frame, MMJJ_16440 fully degraded the larger plasmid with a lower concentration of enzyme (Figure 5, panel 1). One possibility is that the lower GC content allows for increased linearization/degradation of the DNA; however, further investigation is needed to verify.

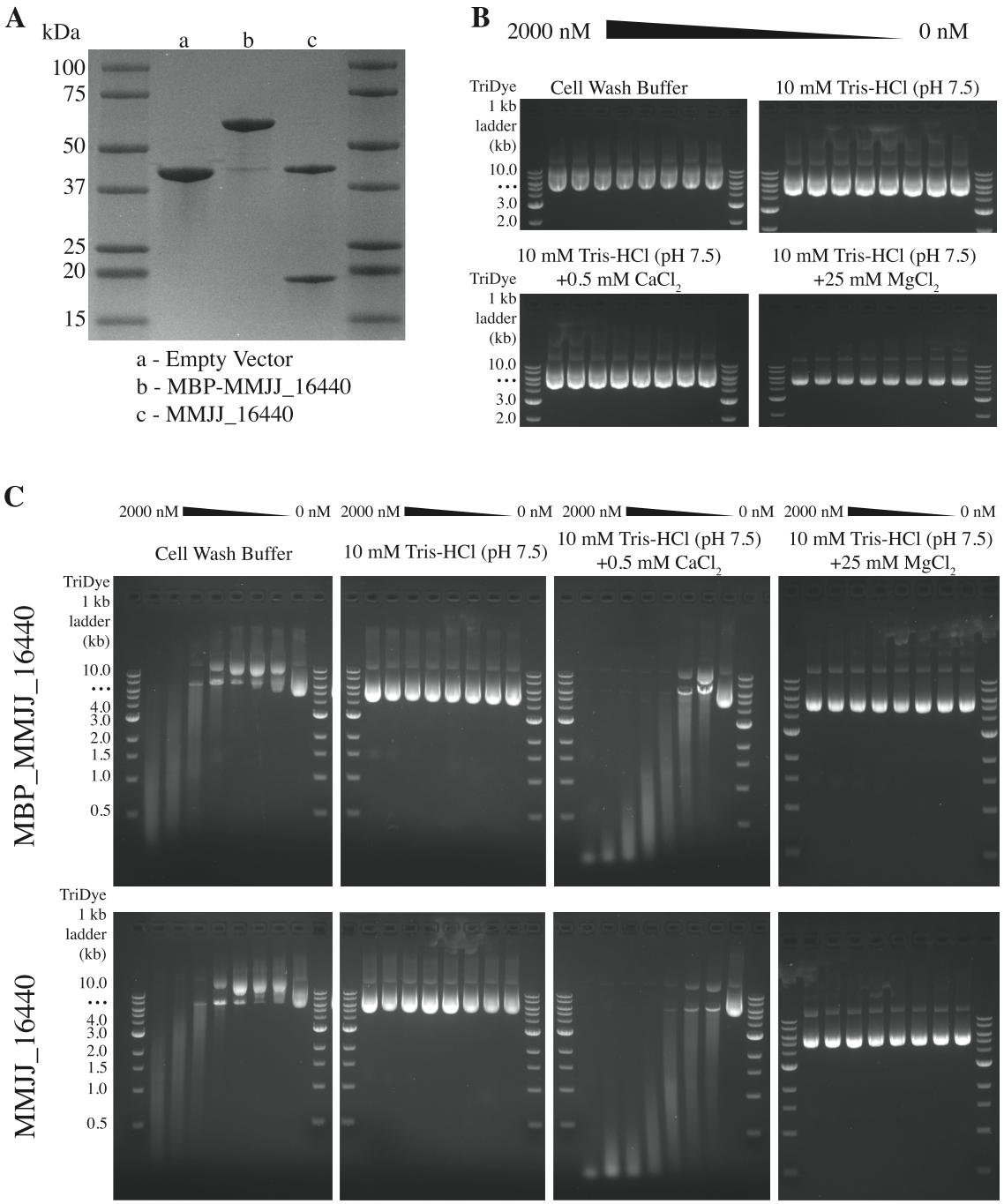

FIGURE 3 | Purification of MMJJ_16440 from *Escherichia coli* and nuclease activity. (A) SDS-PAGE + Coomassie Blue analysis of purified proteins. Empty vector refers to pMAL-C6T which produces the MBP fusion tag (~46 kDa) without an insert. MBP-MMJJ_16440 refers to the fusion construct directly from the amylose column elution. MMJJ_16440 refers to the protein mixture that results after treating MBP-MMJJ_16440 with TEV protease. Bands shown here are dilutions to represent the purity of the sample. (B) Empty vector MBP agarose-based nuclease assay. Enzyme was mixed in a dilution series (highest concentration = 2000 nM then 7 1:2 dilutions and a buffer only control at the end) with pCRUptNeo and incubated at 37°C for 30 min then visualized on a 1% agarose gel. Concentrations of $CaCl_2$ and $MgCl_2$ were chosen to match the concentrations in the wash buffer. (C) Agarose-based nuclease assay comparing the fused MBP-MMJJ_16440 versus the TEV separated MMJJ_16440. Enzymes were normalized based on purity (determined by molecular weight analysis with BioRad Image Lab v4.0.1) and mixed with pCRUptNeo with the highest concentration being 2000 nM, then 6, 1:2 serial dilutions and a buffer only control. Reactions were incubated at 37°C for 30 min then visualized on a 1% agarose gel.

While supercoiled DNA can be fully degraded (Figure 3), we also assayed other DNA substrates. We digested pCRUptNeo with a single blunt end restriction enzyme (ScaI), or a set of enzymes that generated incompatible overhangs (NotI/XbaI). We observed full degradation of DNA, regardless of the substrate provided (Figure 5, panels 2 and 3), but less enzyme was required to degrade linearized DNA (Figure 3C). These data suggest that the linearization of DNA may be the rate-limiting step of the reaction when circular DNA is provided as substrate.

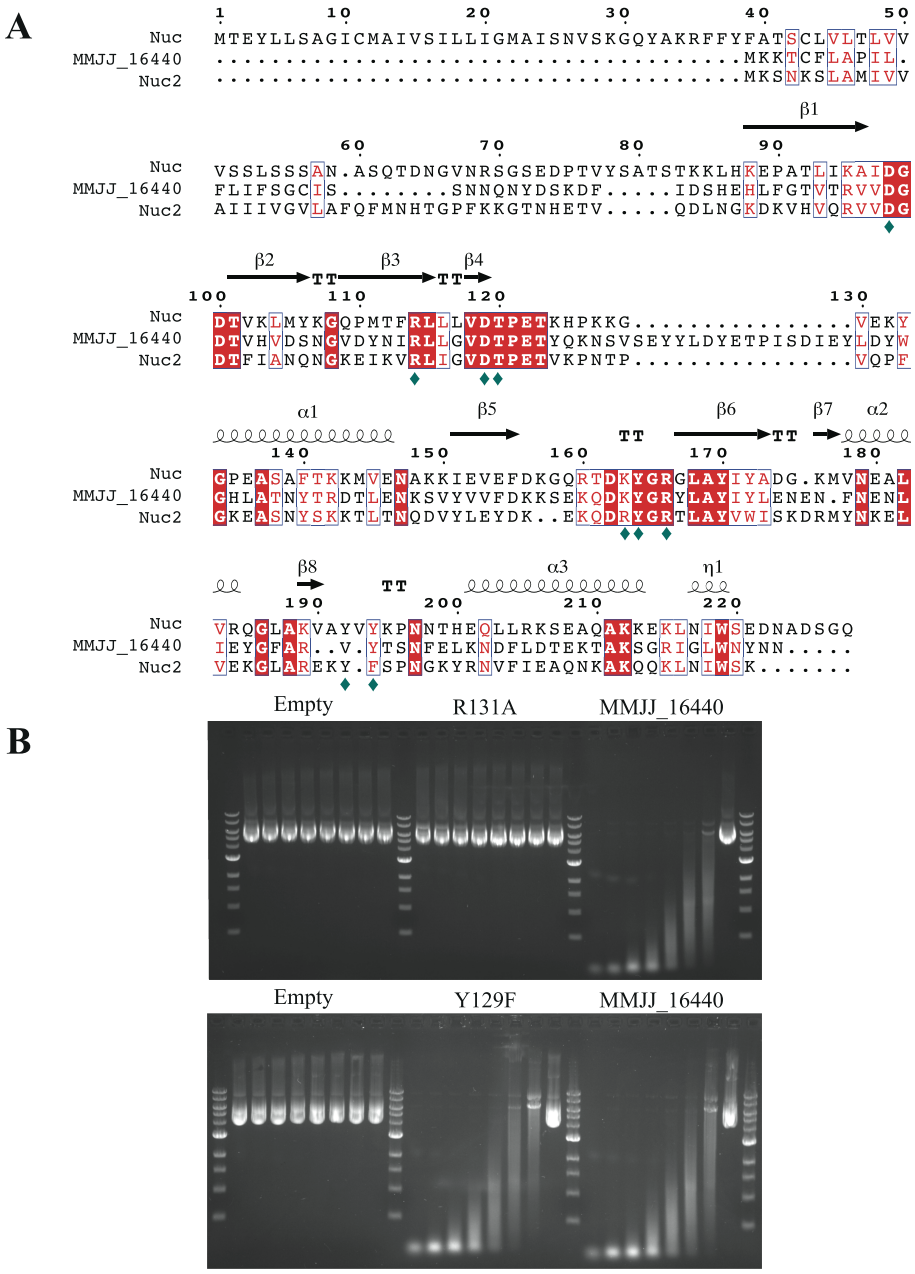

FIGURE 4 | Identification and characterization of MMJJ_16440 catalytic point mutants. (A) Amino acid alignment of Nuc, Nuc2, and MMJJ_16440. The alignment was generated with clustal omega (Madeira et al. 2022) and then the results imported into the ESPript 3 web server (Robert and Gouet 2014) for addition of secondary structure (based on PDB-1EYO to be consistent with (Kiedrowski et al. 2014)). Teal stars below the alignment refer to the nine catalytic residues of Nuc (Cotton, Hazen, and Legg 1979; Kiedrowski et al. 2014). Identical residues are shaded red with white letters, and similar amino acids are in red font surrounded by blue boxes. (B) Agarose assay of MMJJ_16440 catalytic point mutants. Proteins were all freshly purified (see Figure S2 for SDS-PAGE) and subjected to our nuclease assay. Empty refers to MBP purified from pMAL-C6T empty vector. R131A and Y129F refer to the specific point mutants in the MBP-MMJJ_16440Δ2-18. MMJJ_16440 refers to MBP-MMJJ_16440. Enzymes were normalized based on purity (determined by molecular weight analysis with BioRad Image Lab v4.0.1) and mixed with pCRUptNeo with the highest concentration being 2000 nM, then 6, 1:2 serial dilutions and a buffer only control. Reactions were incubated at 37°C for 30 min then visualized on a 1% agarose gel.

2.7 | MMJJ_16440 Is Not Thermostable

Nuc and Nuc2 are thermostable, able to withstand temperatures of 75°C for an hour and still retain activity (Kiedrowski et al. 2014). To determine whether MMJJ_16440 shares this property, we incubated the enzyme in 10 mM Tris–HCl (pH 7.5) at a temperature range of 40°C–64°C for an hour before subjecting heat-treated enzymes to the nuclease assay. We observed complete degradation up to 54.9°C, but no degradation at 59.1°C or higher (Figure 6A). This suggests that the melting temperature (Tm) of the protein must lie somewhere between 54.9°C and 59.1°C. To determine the Tm, we performed a thermal shift assay using the SYPRO orange protein–dye (Huynh and Partch 2015), which binds unfolded protein and produces a fluorescent signal across

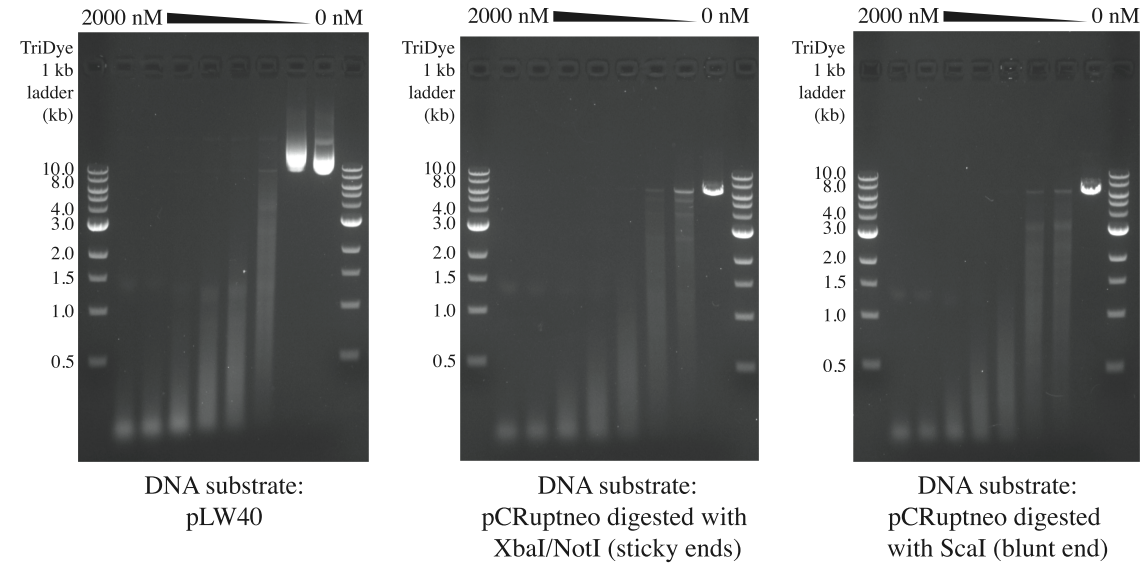

FIGURE 5 | MMJJ_16440 is capable of degrading both dsDNA and ssDNA plasmid DNA. Agarose-based nuclease assays with various dsDNA substrates. Tested DNA substrate was mixed with enzyme for 30 min at 37°C in 20 μL reactions. A dilution series of enzyme from 2000 nM, 6 1:2 dilutions, then a buffer only was tested. pLW40 represents a circular dsDNA of larger size (10.3 kb) than pCRUptNeo (6.6 kb). pCRUptNeo was restriction digested with either XbaI/NotI to generate linear dsDNA with incompatible overhangs or with ScaI to generate blunt ended linear dsDNA. All reactions were visualized on a 1% agarose gel stained with Apex safe DNA stain.

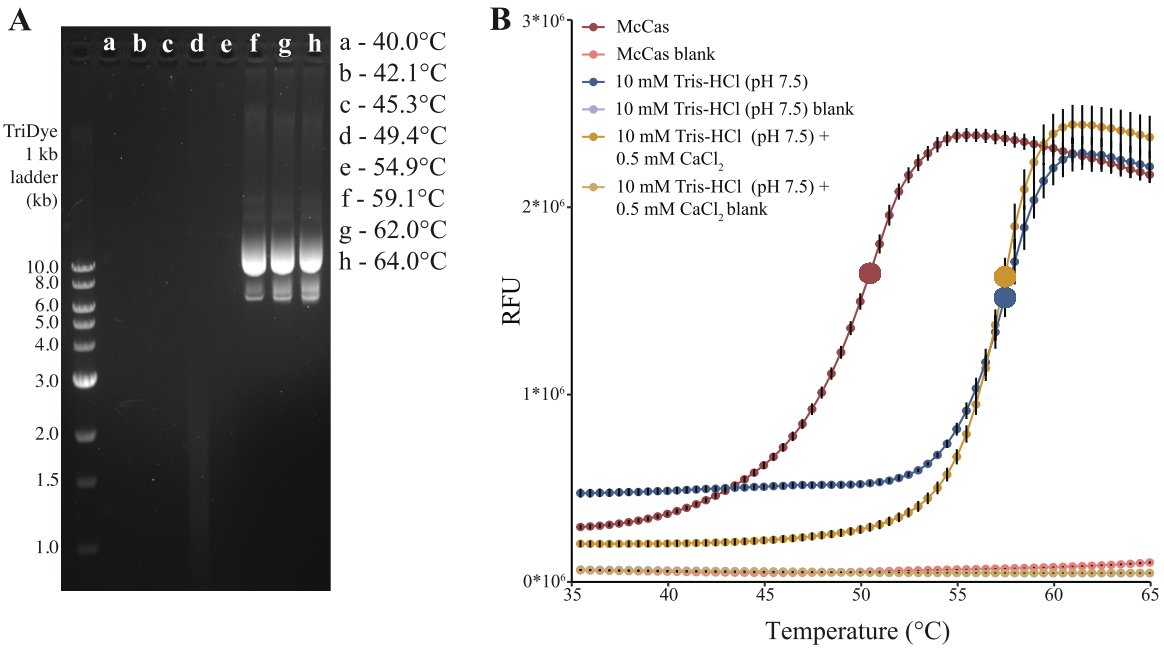

FIGURE 6 | MMJJ_16440 does not have the thermostable properties of Nuc/Nuc2. (A) Agarose-based nuclease assay on heat treated enzyme. 20,000 nM of Mbp-MMJJ_16440 was heat treated between 40°C to 64°C for 1 h then 2000 nM was subjected to our agarose-based nuclease assay. DNA was visualized on a 1% agarose gel stained with Apex safe DNA stain. (B) SYPRO orange Tm assay on Mbp-MMJJ_16440. Melt curves are averages of triplicate reactions and error bars represent one standard deviation around the mean. Protein Tm's, determined using a midpoint Riemann sum with a window of 5 data points, are displayed with large circles. In McCas, the Tm was determined to be 50.5°C while in 10 mM Tris or 10 mM Tris + 0.5 mM CaCl the Tm was 57.5°C.

a temperature gradient. In 10 mM Tris–HCl (pH 7.5) and 10 mM Tris–HCl (pH 7.5) + 0.5 mM $CaCl_2$, the Tm was determined to be 57.5°C. In the culture medium McCas, the Tm was 50.5°C, suggesting that the enzyme is stable under the mesophilic conditions in which *M. maripaludis* grows (Figure 6B).

2.8 | MMJJ_16440 Efficiently Degrades ssDNA

We determined the rate of DNA degradation using a PicoGreen DNA dye-based method, which monitors fluorescent signal based on binding to either dsDNA or ssDNA (Sheppard et al. 2019).

Incubation of PicoGreen-labeled DNA with MMJJ_16440 results in a change in fluorescence over time that can be tracked in real time. To compare MMJJ_16440 to previously reported nucleases, we used the same DNA substrate for the characterization of endonucleases such as DNaseI and ssDNA nucleases such as human Trex2.

MMJJ_16440 activity increased linearly as enzyme concentration increased, suggesting a first-order reaction. The average rate of activity on an 80 bp dsDNA substrate in 10 mM Tris–HCl (pH 7.5) + 0.5 mM $CaCl_2$ was $3.21 \times 10^{-5} \pm 1.88 \times 10^{-5}$ bp $nM^{-1} s^{-1}$ (Figure 7). For comparison, the rate of DNaseI on the same substrate is approximately 1×10^{-3} bp $nM^{-1} s^{-1}$ (Sheppard et al. 2019). To ensure we were achieving comparable results under our laboratory conditions, we additionally performed this assay using the same DNaseI (Promega cat. M6101) as reported in Sheppard et al. (2019) and observed a rate of $2 \times 10^{-3} \pm 1.23 \times 10^{-3}$ bp $nM^{-1} s^{-1}$ (Figure S3).

When 60 bp ssDNA substrate was used, the average rate was $1.26 \times 10^{-3} \pm 1.81 \times 10^{-4}$ bp $nM^{-1} s^{-1}$. For comparison, human Trex2 has a rate between $1.7 \times 10^{-4} - 3.4 \times 10^{-4}$ bp $nM^{-1} s^{-1}$ (Sheppard et al. 2019). The higher rate of ssDNA degradation suggests that ssDNA is the preferred substrate for MMJJ_16440.

2.9 | A Repair Template Increases Transformation Efficiencies in Whole Cells

The entry of ssDNA into cells necessitates either repair to circularized dsDNA (for replicating vectors such as pLW40) or integration into the genome. In the case of replicating vectors, a repair template should increase transformation efficiency. In other words, cells that already contain a plasmid (e.g., pLW40neo) should more effectively take up a similar plasmid with a different antibiotic cassette (e.g., pLW40 that is identical except for containing pur^R instead of neo^R). When WT + pLW40neo was transformed with pLW40, it exhibited a two- to four-fold higher average transformation efficiency ($p = 8.81 \times 10^{-4}$, statistical power of 0.83) as compared to WT transformed with pLW40 (Figure 8A). Furthermore, these experiments were performed in the absence of neomycin to minimize any effects the medium may have on the results. Previously, we have shown that the pLW40neo is stably maintained in *M. maripaludis* (Day et al. 2022) for at least 20 generations, and any attempts to cure the cells of plasmid have been unsuccessful; thus, we predict that the only difference between these genotypes is the presence of a repair template.

An alternative explanation for the increased transformation efficiency in cells containing pLW40neo is that expression of competence machinery is higher in *M. maripaludis* when maintaining a plasmid since positive feedback regulation is common in bacterial competence systems. To test this possibility, we performed an RNA-seq analysis comparing WT and WT + pLW40neo. Of the 1706 genes subjected to differential expression analysis (File S4) with DESeq2, five genes were considered differentially expressed (downregulated in WT + pLW40neo compared with WT) with our chosen cutoffs (Figure S4; File S6). None of these are known to be involved in transformation (File S5) based on our previous characterizations (Fonseca et al. 2020, 2023). This suggests that the increased transformation efficiency is likely due to the presence of a repair template in the cell that facilitates homologous recombination and repair of the incoming ssDNA.

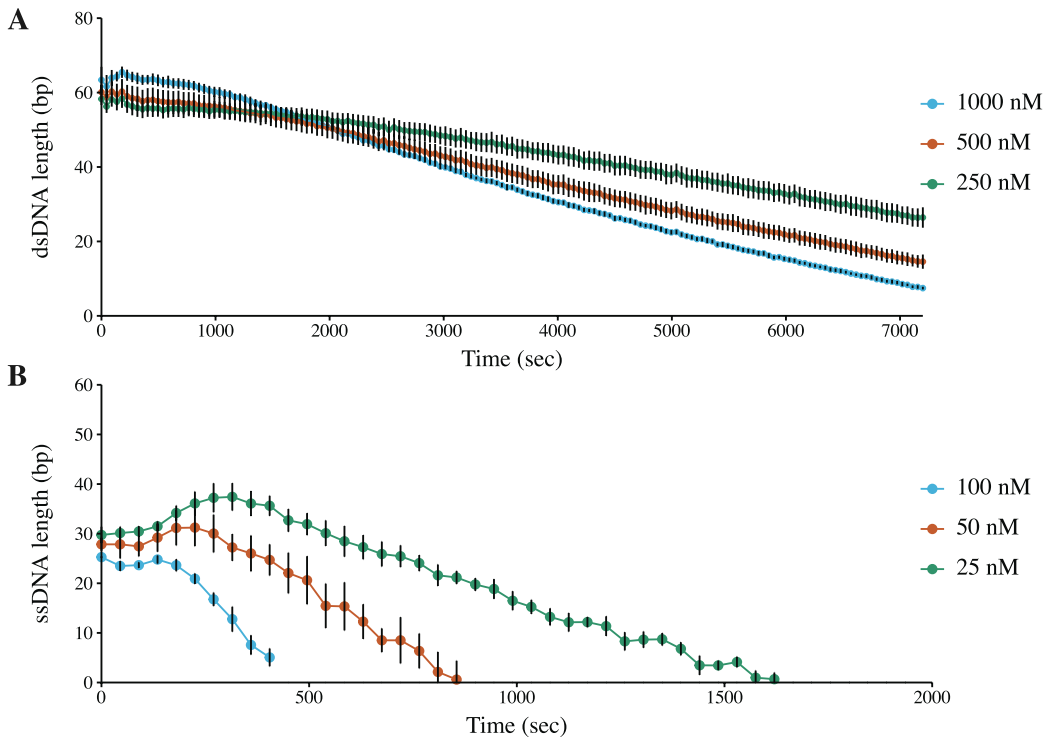

FIGURE 7 | PicoGreen nuclease assay comparing nuclease rates on ssDNA and dsDNA. (A) PicoGreen nuclease assay using an 80 bp dsDNA oligo as the nuclease substrate. Data points are the average of the triplicate measurements and error bars represent one standard deviation around the mean. (B) PicoGreen nuclease assay using a 60 bp ssDNA oligo as the nuclease substrate. Data are the average of triplicate reactions and error bars represent one standard deviation around the mean.

3 | Discussion

Natural transformation is a mechanism by which genetic information can be exchanged between organisms independent of inheritance. To date, the transformation mechanism in archaea has not been described, but several genes essential to transformation have been catalogued (Fonseca et al. 2020, 2023). Here, we characterized a key step of the uptake process, DNA processing. We demonstrate that MMJJ_16440, a predicted extracellular nuclease, is present on the cell surface, is Ca^{2+}-activated, and prefers ssDNA as a substrate. We name this enzyme EcnA (**e**xtracellular, **C**a^{2+}-activated **n**uclease). Based on these observations, we propose the following model for plasmid DNA uptake by *M. maripaludis* (Figure 9). First, circular dsDNA is bound by the Epd pilus and adsorbed to the cell surface. During adsorption, EcnA produces a double-strand break or nick, relaxing/exposing ssDNA. One strand of the DNA is degraded by EcnA, while the other strand is translocated into the cell through a membrane transporter, possibly MMJJ_13030 (Fonseca et al. 2023). Interestingly, MMJJ_13020, which is essential to natural transformation in *M. maripaludis* (Fonseca et al. 2023), is predicted to be membrane-bound (predicted by DeepTMHMM (Hallgren et al. 2022) to have a globular + signal peptide topology) with an extracellular OB-fold nucleic acid–binding domain. OB-fold nucleic acid–binding domains generally bind ssDNA, although examples of dsDNA binding have been documented (Flynn and Zou 2010). Additionally, *in silico* modeling of ComEC from bacteria suggests that it contains an OB-fold ssDNA-binding domain that is on the extracellular face of the transporter. Therefore, we hypothesize that MMJJ_13020 stabilizes one of the strands of the incoming DNA, protecting it from EcnA, before MMJJ_13030 transports it into the cell. In bacteria, ComEA is additionally involved in the binding on the transformed strand of DNA and facilitates the efficient transfer of the DNA from the pilus to ComEC through an atypical helix hairpin helix domain (Ahmed et al. 2022). Determining whether MMJJ_13020 is performing an analogous function in this transfer process warrants further study.

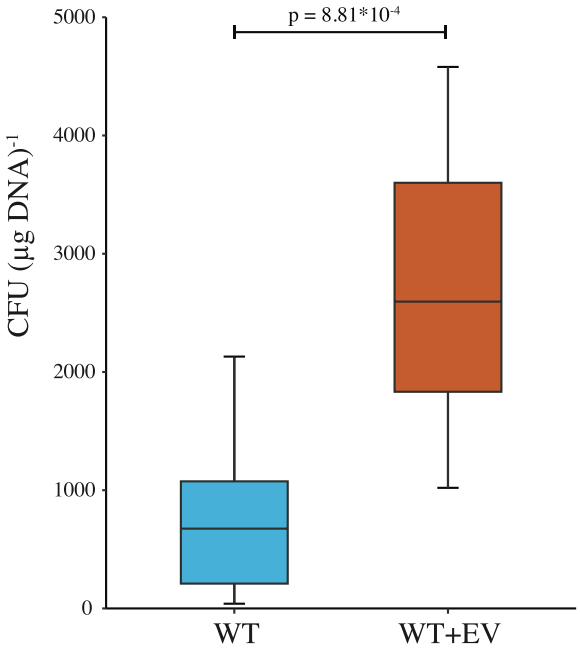

FIGURE 8 | Cells exhibit higher transformation efficiency when a repair template is present. Box plot of *Methanococcus maripaludis* strains naturally transformed with pLW40. Ten biological replicates of either WT (KC13) or KC13 + EV (KC13 + pLW40neo) were transformed with pLW40 following our natural transformation protocol (Fonseca et al. 2020), then plated onto McCas + puromycin agar medium.

This model suggests ssDNA is the substrate for transport into the cell, which is consistent with bacterial transformation. Since a replicating plasmid (pLW40neo), with no ability to recombine into the chromosome can be a substrate, this suggests that the

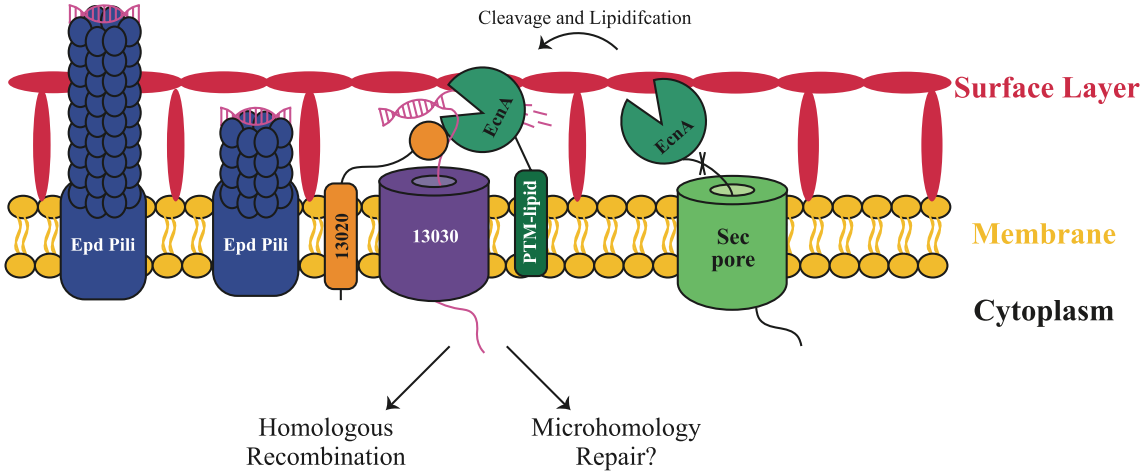

FIGURE 9 | Model of DNA uptake in *Methanococcus maripaludis*. Unnamed proteins are referenced by their locus tag in the format used in Poehlein et al. (MMJJ_XXXXX) (Poehlein et al. 2018). Extracellular DNA is predicted to be bound by extended Epd Pili, then adsorbed to the cell surface during retraction. DNA is processed by the membrane-bound (through a Sec/SPII mechanism; PTM-lipid refers to a lipid post translational modification) nuclease EcnA (MMJJ_16440) which separates the dsDNA into ssDNA. One strand may be stabilized by the membrane protein MMJJ_13020, a putative OB-fold nucleic acid binding protein. The remaining ssDNA is translocated through the membrane, presumably through the TTT family transporter MMJJ_13030. The incoming ssDNA must be repaired through integration into the chromosome (in the case of integrative pCRUptNeo based transformations), homologous recombination with another replicative plasmid/second transformed ssDNA strand (in the case of replicative pLW40/pLW40neo based transformation), or the error prone microhomology-mediated end joining.

incoming DNA must be converted back to circular dsDNA in the cytoplasm. Additionally, the presence of a repair template (such as with WT + pLW40neo transformed with pLW40) significantly increases transformation efficiency (Figure 8), an observation comparable to what is observed in bacterial transformation systems, where longer regions of homology increase transformation efficiency (Zawadzki, Roberts, and Cohan 1995; Majewski et al. 2000; Kung et al. 2013). Given that there are numerous repair machineries (such as RadA/RadB and Mre11/Rad50, which are both involved in homologous recombination) present within *M. maripaludis* the exact mechanism of how this repair occurs is yet to be determined. Should homologous recombination be the main driver of incorporation into the genome (such as in bacteria through RecA) repair of replicative plasmids may occur through the uptake of two ssDNA strands such that they can serve as repair templates for each other.

Characterization of competence nucleases has largely focused on *B. subtilis* (NucA) and *S. pneumoniae* (EndA) (Puyet, Greenberg, and Lacks 1990; Provvedi, Chen, and Dubnau 2001). EcnA is evolutionarily distinct from these nucleases, but we hypothesize that its function in transformation is analogous. Interestingly, *S. aureus* was long considered to be not naturally competent, but recent reports have suggested it can be driven into a competent state during biofilm maturation or after experiencing DNA damage (Morikawa et al. 2012; Cordero et al. 2022; Maree et al. 2022; Costa et al. 2023). Nuc is antagonistic to biofilm initiation due to the degradation of eDNA that stabilizes the biofilm matrix (Kiedrowski et al. 2011; Tang et al. 2011), but the biological role of Nuc2 is unknown. Purified Nuc2 added to cultures has shown reduction in biofilms (Kiedrowski et al. 2014), but in vivo, thicker biofilms have only been observed in *nuc/nuc2* double mutants (Beenken et al. 2012; Yu et al. 2021). Based on these observations, it is plausible that since Nuc2 is membrane-bound, it may serve as the processor of incoming DNA during natural transformation. Unlike *M. maripaludis*, *S. aureus* possesses homologs of ComEC (though *S. aureus* ComEC single mutants have not been tested for competence, disruption of the *comE* operon (contains *comEC*, *comEA*, and *comFA*) in a *sigH* overexpression strain is unable to uptake exogenous DNA (Morikawa et al. 2012)). This suggests that the DNA processing machinery (EndA, NucA, and EcnA) and the DNA uptake machinery (ComEC and MMJJ_13030) evolved separately.

The results presented here are the first characterization of an enzyme required for natural transformation in the archaea. These data provide further clarity to our mechanistic understanding of competence, a process that is suggested to allow microbes to adapt to their environment or maintain the integrity of the genome. These inform on the role of transformation in natural populations and expands our understanding/scope of horizontal gene transfer.

4 | Experimental Procedures

4.1 | Strains, Media, and Growth Conditions

Strains used in this study are listed in Tables S1 and S2. *M. maripaludis* strain JJ was acquired from William Whitman. *E. coli* T7 Expresss *lysY/I*^{q} competent cells (cat. C3013I) were purchased from New England Biolabs. *M. maripaludis* strains were grown in McCas medium at 37°C with agitation as described in Moore and Leigh (2005) with the exceptions in Fonseca et al. (2020). When necessary, the following antibiotics were added to medium at the noted concentrations: neomycin (1 mg mL^{-1} for liquid medium and 0.5 mg mL^{-1} for plates) and puromycin (2.5 μg mL^{-1}). *E. coli* strains were grown in lysogeny broth (LB) or LB + 0.2% glucose. When necessary, ampicillin was added to medium at 100 μg mL^{-1} and incubated at 37°C unless otherwise specified.

4.2 | Plasmid and Strain Construction

Primers are listed in Table S3, and plasmids are listed in Table S4. All PCRs were performed using Phusion High-Fidelity DNA Polymerase in HF buffer (cat. M0531). For expression of genes on pLW40neo-based plasmids, genes were PCR-amplified with a 5′ primer that adds a 20 bp sequence homologous to the region surrounding the NsiI site of pLW40neo and a 3′ primer that adds a linker region, 6× histidine tag, and a 20 bp homology arm to the region surrounding the AscI restriction site of pLW40neo. These sites place the gene under the control of the high expression *Methanococcus voltae* histone promoter (P*hmv*) (Gardner and Whitman 1999). Digested pLW40neo and PCR products were Gibson-assembled (Gibson et al. 2009) using NEBuilder (cat. E2621) then electroporated into electrocompetent *E. coli* strain DH5α. Transformants were selected on lysogeny broth agar medium containing ampicillin and screened for insertion by colony PCR. Colonies positive for insertion were grown in 5 mL of lysogeny broth + ampicillin, and plasmids were purified with the Invitrogen PureLink Quick Plasmid Miniprep Kit (cat. K210010). Purified plasmids were then transferred into *M. maripaludis* strains by the PEG-mediated chemical transformation method described in Tumbula, Makula, and Whitman (1994) with the variations described in Fonseca et al. (2020).

For expression of EcnA and its point mutants on pMAL_C6T, primer design was assisted by the NEBuilder assembly tool (nebuilder.neb.com). Primers were designed to remove amino acids 2–18 and added 20 nucleotides with homology to the regions surrounding the SbfI and AlwNI restriction sites of pMAL-C6T. This site inserts the gene downstream and in frame of *malE* under the control of the inducible *tac* promoter and utilizes the ATG start of the AlwNI site. PCR products and digested pMAL_C6T vector were Gibson-assembled (Gibson et al. 2009) with NEBuilder (cat. E2621). Assemblies were chemically transformed with the High Efficiency Transformation Protocol from NEB (C3013) into T7 Expresss *lysY/I*^{q} competent cells with the exception that lysogeny broth was used instead of SOC medium for the outgrowth. Transformants were plated on lysogeny broth agar medium supplemented with 50 μg mL^{-1} ampicillin. Colonies were screened by colony PCR for insert with the plasmid primers suggested in the NEBExpress MBP Fusion and Purification System protocol (manualE8201; Appendix C 1.2) and by small-scale induction experiments to verify the presence of fusion protein by SDS-PAGE stained with Coomassie.

All plasmid sequences were verified by sequencing with Oxford Nanopore sequencing by Plasmidsaurus (http://www.plasmidsaurus.com).

4.3 | Natural Transformation of *M. maripaludis*

All natural transformations of *M. maripaludis* were performed as described in Fonseca et al. (2020). Transformation efficiency was determined by plating cells on selective medium (McCas + puromycin when transformed with pLW40 and McCas + neomycin when transformed with pLW40neo) and counting the number of colonies per mL of culture. Given that 5 μg of DNA is added to a 5 mL culture, this number also represents CFUs $(\mu g\ DNA)^{-1}$.

4.4 | Phylogenetic Reconstruction of Select Nucleases

The following nucleases amino acid sequences were downloaded from Uniprot.org on 10/23/2023: *M. maripaludis* strain JJ—MMJJ_16440 (A0A2LICCC5), *S. aureus*—Nuc (A0A0H2XHI2), *S. aureus*—Nuc2 (A0A0H2XGE3), *B. subtilus*—NucA (P12667), *S. pneumoniae*—EndA (P0A3S4), and *V. cholerae*—Dns (P08038).

These sequences were then individually run through BlastP in Uniprot.org against the UniprotKB reference proteomes + Swissprot database with the following parameters: Matrix—BLOSUM62, Alignments—500, Scores—500, Exp—0.0001, Filter—F, Gapalign—true, Compstats—F, Align—0, and Stype—protein. All sequences matching these parameters were downloaded as fasta files.

The six fasta files were loaded into the Minnesota Supercomputing Institute (MSI) server where they were merged and deduplicated (on name and sequence) into a single fasta file (File S1). The surviving 1959 sequences were subject to multiple sequence alignment with Muscle v3.8.31 (Edgar 2004) with the maxiters flag set to 2 as suggested by the software manual for alignment of large datasets. The resulting alignment was then trimmed with trimAl using the automated1 flag (Capella-Gutiérrez, Silla-Martínez, and Gabaldón 2009). Trimmed alignments were then used for tree construction with FastTree v2.1.8 (Price, Dehal, and Arkin 2009, 2010) and exported as a tree file in Newick format (File S2). The tree file was then uploaded into the interactive tree of life (iTol) web browser (Letunic and Bork 2021) (https://itol.embl.de/) for visualization. Branch labels were hidden, and the tree type was set to unrooted. The six input nuclease sequences were then identified by their accession number using iTol's branch search tool, and their relative positive was marked with a red dot.

4.5 | FRET-Based Nuclease Assay

The FRET-based nuclease assay methods were adapted for use in *M. maripaludis* based on the protocols described previously (Kiedrowski et al. 2011, 2014). Briefly, a freshly grown 5 mL culture of each strain in stationary phase was repressurized to 207 kPa with 80%:20% N_2:CO_2, then centrifuged at 2500×*g* for 20 min. Balch tubes were then released of their pressure and opened. The supernatant of each culture was transferred to a 5-mL syringe with a 0.2 μm PVDF membrane filter and filtered to remove unpelleted cells into a 3 k MWCO concentrator (cat. 885626). Concentrators were then spun at 4000×*g* at 4°C until the volume remaining was approximately 500 μL. Pellets were then resuspended in 1 mL of *Methanococcus* wash buffer (10 mM Tris–HCl pH 7.5, 22 g/L NaCl, 0.33 g/L KCl, 2.75 g/L $MgCl_2{\cdot}6H_20$, 3.45 g/L $MgSO_4{\cdot}7H_20$, 0.14 g/L $CaCl_2{\cdot}2H_20$) and transferred to 1.5-mL microcentrifuge tubes. Cells were washed 2 times in 1 mL of wash buffer through centrifugation at 2500×*g* for 20 min in a tabletop centrifuge and decanting the supernatant with a pipette. Washed pellets were resuspended in 250 μL of wash buffer.

50 μL of either washed whole-cells or concentrated secretomes was then mixed in black flat bottom 96-well plates with 1 μL of 100 μM Prime-Time qPCR probe (Kiedrowski et al. 2011) (final concentration adjusted to 2 μM to account for the high background fluorescence in the secretome samples) in quadruplicate and fluorescence was measured every 2 min for 1 h in a Spectramax M2^e plate reader set to 37°C with 10 flashes per well, excitation 552 nm, emission 580 nm, and shaking before each read.

4.6 | Expression and Purification of EcnA

All expression and purification of EcnA was performed using the NEBExpress MBP Fusion and Purification System (cat. E8200). In summary, T7 Express *lysY/I^q* harboring our expression constructs were inoculated from freezer stocks into LB + ampicillin 5 mL of cultures and grown overnight at 37°C with agitation. The next day, cultures were subinoculated into 2–4500 mL LB + 0.2% glucose + ampicillin with 1–5 mL and grown at 37°C with agitation until an OD_{600} of ~0.4. Flasks were then induced by the addition of IPTG (final concentration 0.3 mM) and grown for an additional 2 h at 37°C with agitation. Induced cells were harvested by centrifugation at 4000×*g* for 20 min, and the supernatant was discarded. Cell pellets were resuspended in 25 mL of column buffer (20 mM Tris–HCl pH 7.5, 200 mM NaCl, 1 mM EDTA) and frozen at −20°C.

Frozen cell suspensions were then thawed at room temperature and sonicated on ice with a Qsonica XL-2000 series tip sonicator by pulsing for 15 s on, 15 s off, 5–10 times. Cell lysates were then centrifuged at 20,000×*g* for 20 min at 4°C to remove the cell debris. Supernatants were separated from the debris and diluted 1:5 in column buffer before loading into a 10 mL bed volume Amylose resin column by gravity flow. Column was then washed with 2 L of column buffer and eluted with 100 mL of column buffer + 10 mM d-(+)-maltose monohydrate (cat. A16266.22) collected as a single fraction. The eluate was subsequently concentrated in 10 k MWCO concentrators (cat. 88517) and buffer exchanged into 10 mM Tris–HCl pH 7.5 by centrifugation at 4000×*g* at 4°C. Concentration was determined by Bradford (Bradford 1976) using the Coomassie protein assay reagent (cat. 1856209).

To separate EcnA from the MBP tag, 500 μL TEV reactions were performed at room temperature from 10 h to overnight. Reactions were routinely performed with 15 μL of TEV protease (cat. P8112S), and protease activity was monitored for complete digestion by SDS-PAGE stained with Coomassie. Completely digested protein was diluted to 5 mL with 10 mM Tris–HCl pH 7.5 then loaded by gravity flow into a 1 mL bed volume his

resin column preequilibrated with 10 mM Tris–HCl pH 7.5 and the flow through was collected. The column was additionally washed with 5 mL of 10 mM Tris–HCl pH 7.5 and the flow was collected. The 10 mL flow was then concentrated to ~500 μL in a 3 k MWCO Concentrator (Thermo Scientific cat. 885626) by centrifugation at 4000×*g* at 4°C and concentration was determined by Bradford assay (Bradford 1976). Purity of EcnA was assessed by SDS-PAGE stained with Coomassie and analyzed with the molecular weight analysis tool in BioRad Image Lab v4.0.1. Routinely, EcnA consisted of ~40%–60% of the protein mixture and the concentration used in downstream experiments was adjusted to account for the purity.

4.7 | Agarose-Based Nuclease Assay

Purified enzyme was first diluted to a 10× assay concentration of 20,000 nM in 10 mM Tris–HCl pH 7.5. Subsequently, six 1:2 dilutions were created and an empty tube containing buffer only was set up. 20 μL nuclease reactions was set up either by mixing 2 μL 10× buffer (100 mM Tris–HCl and, when necessary, 5 mM $CaCl_2$ or 250 mM $MgCl_2$) or 10 μL or 2× cell wash buffer with 1000 ng of DNA, then filled to 18 μL with water. Reactions were initiated with 2 μL of the 10× enzyme for a final concentration of 2000, 1000, 500, 250, 125, 62.5, 31.25, or 0 nM of enzyme respectively and mixed by flicking/brief centrifugation in a tabletop centrifuge. Reactions were then incubated at 37°C for 30 min before being stopped by addition of 2.2 μL of 10× Tris/Glycine/SDS running buffer (cat. 1610772). 4.4 μL of 6× loading dye was then added to the reaction and the entire contents were subject to agarose gel electrophoresis in a 1% agarose gel stained with apex safe DNA stain (cat. 20-278). Gels were then imaged and analyzed using BioRad Image Lab v4.0.1.

4.8 | EcnA Tm Determination

For agarose-based Tm determination, eight tubes containing 20,000 nM of enzyme were subject to 1 h of incubation in a BioRad S1000 thermal cycler using the gradient function set from 40°C to 64°C. 2 μL heat treated enzyme was then transferred to 20 μL nuclease reactions, incubated, and visualized using the same methods described above.

Further Tm determination was performed using the thermal shift assay described in Huynh and Partch (2015). Briefly, enzyme was diluted to 20 μM in 1× buffer (McCas, 10 mM Tris–HCl, 10 mM Tris–HCl + 0.5 mM $CaCl_2$) to equilibrate it to the tested buffer. 50 μL Tm reactions was then set up in triplicate in 96-well qPCR plates such that the final reaction contained 1× buffer, 5 μM enzyme (or 0 μM, and 20× SYPRO orange (cat. S6650)). Plates were sealed with optically clear film and centrifuged for 1 min at 800 RPM to remove bubbles. The thermal shift assay was then performed using the StepOne Melt-curve experiment protocol in a StepOnePlus real-time thermocycler with the following parameters: Dye-Other, standard run-time, Reporter—ROX, Quencher—none, initial hold for 3.5 min at 25°C, ramp from 25°C to 95°C at 0.5°C/30 s, and final hold for 3.5 min at 95°C. Normalized data was then exported from StepOne for analysis in excel/R.

4.9 | Picogreen Nuclease Assay

To determine the EcnA's nuclease rate, the assay described in Sheppard et al. (2019) was utilized using the DNA oligos RCOL556/557/609/610/611. Briefly, the 100 μL nuclease reactions were set up in black flat bottom 96-well plates and contained a 10 mM Tris–HCl + 0.5 mM $CaCl_2$, 50 nM DNA substrate, 50 μL of Picogreen diluted 1:200 in 10 mM Tris–HCl pH 7.5, 1 mM EDTA, and 40% (v/v) glycerol. Reactions were then initiated by the addition of enzyme then immediately transferred to a Spectramax M2^e plate reader pre heated to 37°C. Samples were read every 45 s from 1 to 2 h with the following settings: excitation—490 nm, emission—525 nm, cutoff—515 nm, 20 flashes/read, and shake before each read.

4.10 | Purification, Sequencing, and Differential Expression Analysis of RNA

Strains KC13 and KC19 were grown in triplicate in McCas without the addition of any antibiotics overnight until stationary phase. Cultures were then fed with 276 kPa 80:20 H_2:CO_2 and allowed to shake at 37°C for an hour to mimic the DNA uptake observed in our natural transformation protocol. 1 mL of culture was then harvested by centrifugation in a Fischer scientific accuSpin Micro 17 centrifuge at max speed for 1 min in an oxic environment. RNA was then extracted using the RNA Clean and Concentrator-25 kit (cat. R1017) and finally eluted in 50 μL of DNase/RNase-Free Water. Concentration of RNA was determined using a Spectramax M2^e plate reader and the samples were frozen at −80°C. The top two samples for each strain (based on concentration, 260/280, and 260/230 values) were then shipped on dry ice to SeqCenter for RNA sequencing and initial analysis.

Samples were DNAse treated with Invitrogen DNAse (RNAse free). Library preparation was performed using Illumina's Stranded Total RNA Prep Ligation with Ribo-Zero Plus kit and 10 bp IDT for Illumina indices. Sequencing was done on a NextSeq2000 giving 2 × 51 bp reads. Quality control and adapter trimming was performed with trimmomatic version 0.33 (Bolger, Lohse, and Usadel 2014) (leading:3 trailing:3 slidingwindow:4:15 minlen:36). Read mapping was performed with Bowtie2 (v 2.3.4.1) with default parameters against *M. maripaludis* strain JJ's reference genome (accession NZ_CP026606). Read quantification was performed using Subread's featureCounts functionality (Liao, Smyth, and Shi 2014). Quantified counts were then loaded into R and analyzed/visualized using the DESeq2 package (Love, Huber, and Anders 2014). First, genes with less than 10 counts were removed from the dataset. Remaining genes were then analyzed with the DESeq function of DESeq2 with the lfcThreshold = 1 and the alpha = 0.05. Data were visualized with the plotMA function of DESeq2 (Figure S4). Files summarizing the data can be accessed as supplemental Files S4–S6.

Author Contributions

Dallas R. Fonseca: conceptualization, data curation, formal analysis, investigation, methodology, visualization, writing – original draft, writing – review and editing, software. **Leslie A. Day:** conceptualization,

data curation, methodology, visualization, software, writing – review and editing. **Kathryn K. Crone:** conceptualization, methodology, writing – review and editing. **Kyle C. Costa:** conceptualization, funding acquisition, project administration, resources, supervision, writing – review and editing.

Acknowledgments

We thank Dr. Sudipta Shaw for assistance with the thermal shift assay methodology. This work was supported by the National Science Foundation under grant number MCB-2148165.

Conflicts of Interest

The authors declare no conflicts of interest.

Data Availability Statement

The data that supports the findings of this study are available in the supplementary material of this article.

References

Ahmed, I., J. Hahn, A. Henrickson, et al. 2022. "Structure-Function Studies Reveal ComEA Contains an Oligomerization Domain Essential for Transformation in Gram-Positive Bacteria." *Nature Communications* 13: 7724.

Averhoff, B., L. Kirchner, K. Pfefferle, and D. Yaman. 2021. "Natural Transformation in Gram-Negative Bacteria Thriving in Extreme Environments: From Genes and Genomes to Proteins, Structures and Regulation." *Extremophiles* 25: 425–436.

Avery, O. T., C. M. Macleod, and M. McCarty. 1944. "Studies on the Chemical Nature of the Substance Inducing Transformation of Pneumococcal Types: Induction of Transformation by a Desoxyribonucleic Acid Fraction Isolated From Pneumococcus Type III." *Journal of Experimental Medicine* 79: 137–158.

Beenken, K. E., H. Spencer, L. M. Griffin, and M. S. Smeltzer. 2012. "Impact of Extracellular Nuclease Production on the Biofilm Phenotype of *Staphylococcus aureus* Under *In Vitro* and *In Vivo* Conditions." *Infection and Immunity* 80: 1634–1638.

Bolger, A. M., M. Lohse, and B. Usadel. 2014. "Trimmomatic: A Flexible Trimmer for Illumina Sequence Data." *Bioinformatics* 30: 2114–2120.

Bradford, M. M. 1976. "A Rapid and Sensitive Method for the Quantitation of Microgram Quantities of Protein Utilizing the Principle of Protein-Dye Binding." *Analytical Biochemistry* 72: 248–254.

Capella-Gutiérrez, S., J. M. Silla-Martínez, and T. Gabaldón. 2009. "trimAl: A Tool for Automated Alignment Trimming in Large-Scale Phylogenetic Analyses." *Bioinformatics* 25: 1972–1973.

Cordero, M., J. García-Fernández, I. C. Acosta, et al. 2022. "The Induction of Natural Competence Adapts Staphylococcal Metabolism to Infection." *Nature Communications* 13: 1525.

Costa, M. O. C. E., A. P. B. do Nascimento, Y. C. Martins, et al. 2023. "The Gene Regulatory Network of *Staphylococcus aureus* ST239-SCCmecIII Strain Bmb9393 and Assessment of Genes Associated With the Biofilm in Diverse Backgrounds." *Frontiers in Microbiology* 13: 1049819.

Cotton, F. A., E. E. Hazen, and M. J. Legg. 1979. "Staphylococcal Nuclease: Proposed Mechanism of Action Based on Structure of Enzyme—Thymidine 3′,5′-Bisphosphate—Calcium ion Complex at 1.5-Å Resolution." *Proceedings of the National Academy of Sciences of the United States of America* 76: 2551–2555.

Day, L. A., E. L. Kelsey, D. R. Fonseca, and K. C. Costa. 2022. "Interspecies Formate Exchange Drives Syntrophic Growth of *Syntrophotalea carbinolica* and *Methanococcus maripaludis*." *Applied and Environmental Microbiology* 88: e0115922.

Edgar, R. C. 2004. "MUSCLE: Multiple Sequence Alignment With High Accuracy and High Throughput." *Nucleic Acids Research* 32: 1792–1797.

Flynn, R. L., and L. Zou. 2010. "Oligonucleotide/Oligosaccharide-Binding (OB) Fold Proteins: A Growing Family of Genome Guardians." *Critical Reviews in Biochemistry and Molecular Biology* 45: 266–275.

Fonseca, D. R., M. F. A. Halim, M. P. Holten, and K. C. Costa. 2020. "Type IV-Like Pili Facilitate Transformation in Naturally Competent Archaea." *Journal of Bacteriology* 202: e00355-20.

Fonseca, D. R., M. B. Loppnow, L. A. Day, E. L. Kelsey, M. F. Abdul Halim, and K. C. Costa. 2023. "Random Transposon Mutagenesis Identifies Genes Essential for Transformation in *Methanococcus maripaludis*." *Molecular Genetics and Genomics* 298: 537–548.

Gardner, W. L., and W. B. Whitman. 1999. "Expression Vectors for *Methanococcus maripaludis*: Overexpression of Acetohydroxyacid Synthase and Beta-Galactosidase." *Genetics* 152: 1439–1447.

Gibson, D. G., L. Young, R.-Y. Chuang, J. C. Venter, C. A. Hutchison, and H. O. Smith. 2009. "Enzymatic Assembly of DNA Molecules up to Several Hundred Kilobases." *Nature Methods* 6: 343–345.

Gophna, U., and N. Altman-Price. 2022. "Horizontal Gene Transfer in Archaea-From Mechanisms to Genome Evolution." *Annual Review of Microbiology* 76: 481–502.

Hallgren, J., K. D. Tsirigos, M. D. Pedersen, et al. 2022. "DeepTMHMM Predicts Alpha and Beta Transmembrane Proteins Using Deep Neural Networks." 2022.04.08.487609 https://www.biorxiv.org/content/10.1101/2022.04.08.487609v1.

Huynh, K., and C. L. Partch. 2015. "Current Protocols in Protein Science." *Current Protocols in Protein Science* 79: 28.9.1–28.9.14.

Johnston, C. H. G., R. Hope, A.-L. Soulet, M. Dewailly, D. De Lemos, and P. Polard. 2023. "The RecA-Directed Recombination Pathway of Natural Transformation Initiates at Chromosomal Replication Forks in the Pneumococcus." *Proceedings of the National Academy of Sciences of the United States of America* 120: e2213867120.

Kelley, L., S. Mezulis, C. Yates, et al. 2015. "The Phyre2 Web Portal for Protein Modeling, Prediction and Analysis." *Nature Protocols* 10: 845–858.

Kiedrowski, M. R., H. A. Crosby, F. J. Hernandez, C. L. Malone, J. O. McNamara, and A. R. Horswill. 2014. "*Staphylococcus aureus* Nuc2 is a Functional, Surface-Attached Extracellular Nuclease." *PLoS One* 9: e95574.

Kiedrowski, M. R., J. S. Kavanaugh, C. L. Malone, et al. 2011. "Nuclease Modulates Biofilm Formation in Community-Associated Methicillin-Resistant *Staphylococcus aureus*." *PLoS One* 6: e26714.

Kung, S. H., A. C. Retchless, J. Y. Kwan, and R. P. P. Almeida. 2013. "Effects of DNA Size on Transformation and Recombination Efficiencies in *Xylella fastidiosa*." *Applied and Environmental Microbiology* 79: 1712–1717.

Letunic, I., and P. Bork. 2021. "Interactive Tree of Life (iTOL) v5: An Online Tool for Phylogenetic Tree Display and Annotation." *Nucleic Acids Research* 49: W293–W296.

Liao, Y., G. K. Smyth, and W. Shi. 2014. "featureCounts: An Efficient General Purpose Program for Assigning Sequence Reads to Genomic Features." *Bioinformatics* 30: 923–930.

Lipscomb, G. L., K. Stirrett, G. J. Schut, et al. 2011. "Natural Competence in the Hyperthermophilic Archaeon *Pyrococcus furiosus* Facilitates Genetic Manipulation: Construction of Markerless Deletions of Genes Encoding the Two Cytoplasmic Hydrogenases." *Applied and Environmental Microbiology* 77: 2232–2238.

Lo Scrudato, M., and M. Blokesch. 2012. "The Regulatory Network of Natural Competence and Transformation of *Vibrio cholerae*." *PLoS Genetics* 8: e1002778.

Love, M. I., W. Huber, and S. Anders. 2014. "Moderated Estimation of Fold Change and Dispersion for RNA-Seq Data With DESeq2." *Genome Biology* 15: 550.

Madeira, F., M. Pearce, A. R. N. Tivey, et al. 2022. "Search and Sequence Analysis Tools Services From EMBL-EBI in 2022." *Nucleic Acids Research* 50: W276–W279.

Maier, B. 2020. "Competence and Transformation in *Bacillus subtilis*." *Current Issues in Molecular Biology* 37: 57–76.

Majewski, J., P. Zawadzki, P. Pickerill, F. M. Cohan, and C. G. Dowson. 2000. "Barriers to Genetic Exchange Between Bacterial Species: *Streptococcus pneumoniae* Transformation." *Journal of Bacteriology* 182: 1016–1023.

Maree, M., L. T. Thi Nguyen, R. L. Ohniwa, M. Higashide, T. Msadek, and K. Morikawa. 2022. "Natural Transformation Allows Transfer of SCCmec-Mediated Methicillin Resistance in *Staphylococcus aureus* Biofilms." *Nature Communications* 13: 2477.

Moon, A. F., M. Midon, G. Meiss, A. Pingoud, R. E. London, and L. C. Pedersen. 2011. "Structural Insights Into Catalytic and Substrate Binding Mechanisms of the Strategic EndA Nuclease From *Streptococcus pneumoniae*." *Nucleic Acids Research* 39: 2943–2953.

Moore, B. C., and J. A. Leigh. 2005. "Markerless Mutagenesis in *Methanococcus maripaludis* Demonstrates Roles for Alanine Dehydrogenase, Alanine Racemase, and Alanine Permease." *Journal of Bacteriology* 187: 972–979.

Morikawa, K., A. J. Takemura, Y. Inose, et al. 2012. "Expression of a Cryptic Secondary Sigma Factor Gene Unveils Natural Competence for DNA Transformation in *Staphylococcus aureus*." *PLoS Pathogens* 8: e1003003.

Patel, G. B., J. H. E. Nash, B. J. Agnew, and G. D. Sprott. 1994. "Natural and Electroporation-Mediated Transformation of *Methanococcus voltae* Protoplasts." *Applied and Environmental Microbiology* 60: 903–907.

Piepenbrink, K. H. 2019. "DNA Uptake by Type IV Filaments." *Frontiers in Molecular Biosciences* 6: 1.

Pimentel, Z. T., and Y. Zhang. 2018. "Evolution of the Natural Transformation Protein, ComEC, in Bacteria." *Frontiers in Microbiology* 9: 2980.

Poehlein, A., D. Heym, V. Quitzke, J. Fersch, R. Daniel, and M. Rother. 2018. "Complete Genome Sequence of the *Methanococcus maripaludis* Type Strain JJ (DSM 2067), a Model for Selenoprotein Synthesis in Archaea." *Genome Announcements* 6: e00237-18.

Pohlschroder, M., F. Pfeiffer, S. Schulze, and M. F. A. Halim. 2018. "Archaeal Cell Surface Biogenesis." *FEMS Microbiology Reviews* 42: 694–717.

Price, M. N., and A. P. Arkin. 2017. "PaperBLAST: Text Mining Papers for Information About Homologs." *mSystems* 2: e00039-17.

Price, M. N., P. S. Dehal, and A. P. Arkin. 2009. "FastTree: Computing Large Minimum Evolution Trees With Profiles Instead of a Distance Matrix." *Molecular Biology and Evolution* 26: 1641–1650.

Price, M. N., P. S. Dehal, and A. P. Arkin. 2010. "FastTree 2—Approximately Maximum-Likelihood Trees for Large Alignments." *PLoS One* 5: e9490.

Provvedi, R., I. Chen, and D. Dubnau. 2001. "NucA is Required for DNA Cleavage During Transformation of *Bacillus subtilis*." *Molecular Microbiology* 40: 634–644.

Puyet, A., B. Greenberg, and S. A. Lacks. 1990. "Genetic and Structural Characterization of *endA*: A Membrane-Bound Nuclease Required for Transformation of *Streptococcus pneumoniae*." *Journal of Molecular Biology* 213: 727–738.

Robert, X., and P. Gouet. 2014. "Deciphering Key Features in Protein Structures With the New ENDscript Server." *Nucleic Acids Research* 42: W320–W324.

Sato, T., T. Fukui, H. Atomi, and T. Imanaka. 2003. "Targeted Gene Disruption by Homologous Recombination in the Hyperthermophilic Archaeon *Thermococcus kodakaraensis* KOD1." *Journal of Bacteriology* 185: 210–220.

Schultz, D., P. G. Wolynes, E. B. Jacob, and J. N. Onuchic. 2009. "Deciding Fate in Adverse Times: Sporulation and Competence in *Bacillus subtilis*." *Proceedings of the National Academy of Sciences of the United States of America* 106: 21027–21034.

Sheppard, E. C., S. Rogers, N. J. Harmer, and R. Chahwan. 2019. "A Universal Fluorescence-Based Toolkit for Real-Time Quantification of DNA and RNA Nuclease Activity." *Scientific Reports* 9: 8853.

Sun, Y., E. E. Bernardy, B. K. Hammer, and T. Miyashiro. 2013. "Competence and Natural Transformation in Vibrios." *Molecular Microbiology* 89: 583–595. https://doi.org/10.1111/mmi.12307.

Tang, J., M. Kang, H. Chen, et al. 2011. "The Staphylococcal Nuclease Prevents Biofilm Formation in *Staphylococcus aureus* and Other Biofilm-Forming Bacteria." *Science China. Life Sciences* 54: 863–869.

Teufel, F., J. J. Almagro Armenteros, A. R. Johansen, et al. 2022. "SignalP 6.0 Predicts all Five Types of Signal Peptides Using Protein Language Models." *Nature Biotechnology* 40: 1023–1025.

Tumbula, D. L., R. A. Makula, and W. B. Whitman. 1994. "Transformation of *Methanococcus maripaludis* and Identification of a Pst I-Like Restriction System." *FEMS Microbiology Letters* 121: 309–314.

van Sinderen, D., R. Kiewiet, and G. Venema. 1995. "Differential Expression of Two Closely Related Deoxyribonuclease Genes, *nucA* and *nucB*, in *Bacillus subtilis*." *Molecular Microbiology* 15: 213–223.

Vosman, B., J. Kooistra, J. Olijve, and G. Venema. 1987. "Cloning in *Escherichia coli* of the Gene Specifying the DNA-Entry Nuclease of *Bacillus subtilis*." *Gene* 52: 175–183.

Vosman, B., G. Kuiken, J. Kooistra, and G. Venema. 1988. "Transformation in *Bacillus subtilis*: Involvement of the 17-Kilodalton DNA-Entry Nuclease and the Competence-Specific 18-Kilodalton Protein." *Journal of Bacteriology* 170: 3703–3710.

Wagner, A., R. J. Whitaker, D. J. Krause, et al. 2017. "Mechanisms of Gene Flow in Archaea." *Nature Reviews. Microbiology* 15: 492–501.

Worrell, V. E., D. P. Nagle, D. McCarthy, and A. Eisenbraun. 1988. "Genetic Transformation System in the Archaebacterium *Methanobacterium thermoautotrophicum Marburg*." *Journal of Bacteriology* 170: 653–656.

Yu, J., F. Jiang, F. Zhang, et al. 2021. "Thermonucleases Contribute to *Staphylococcus aureus* Biofilm Formation in Implant-Associated Infections—A Redundant and Complementary Story." *Frontiers in Microbiology* 12: 687888.

Zawadzki, P., M. S. Roberts, and F. M. Cohan. 1995. "The Log-Linear Relationship Between Sexual Isolation and Sequence Divergence in *Bacillus* Transformation is Robust." *Genetics* 140: 917–932.

Supporting Information

Additional supporting information can be found online in the Supporting Information section.